Nonlinear Dyn (2020) 101:2629–2644
https://doi.org/10.1007/s11071-020-05875-1

ORIGINAL PAPER

Lissajous and halo orbits in the restricted three-body problem by normalization method

Tong Luo · Giuseppe Pucacco · Ming Xu

Received: 13 November 2019 / Accepted: 1 August 2020 / Published online: 11 August 2020

Abstract We perform an analytical study of the Lissajous and halo orbits around collinear points L_1 and L_2 in a spatial circular restricted three-body problem of an arbitrary value of the mass ratio. Using a canonical transformation procedure, we generate complete and resonant normal forms through reduction to center manifolds. The coefficients in the normal forms are explicitly expressed as functions of mass ratio for the first time so that one can evaluate the energy level at which bifurcation of halo orbit takes place. Another contribution of this paper is giving the analytical solutions of Lissajous and halo orbits in the initial synodic reference system through the inverse transformation of normalization. The analytical results are the series form of normalized action-angle variables, and their coefficients are also explicitly expressed as functions of mass ratio. Finally, comparison results demonstrate that the solutions for a Lissajous orbit derived through normalization method and Lindstedt–Poincaré method are completely the same, while the solutions for a halo orbit derived through these two methods are different but have the roughly equal accuracy.

Keywords Halo orbits · Lissajous orbits · Spatial circular restricted three-body problem · Normalization method · Lindstedt–Poincaré method

1 Introduction

Spatial circular restricted three-body problem (SCR3BP) is a fundamental model to describe the motion of a small body affected by the gravitational attraction of two primaries. Different values of the mass ratio μ ($0 < \mu \leq 1/2$) of the primaries correspond to different celestial systems, such as the Earth–Moon case and the Sun–Earth case. On the line connecting the two primaries exist three collinear equilibrium points [1], which are linearly unstable for arbitrary value of μ. However, Lyapunov's center theory [2] guarantees each collinear point can generate a pair of periodic orbit families, to which we refer as the planar and the vertical Lyapunov families. Quasiperiodic orbits, which form the so-called

Electronic supplementary material The online version of this article (https://doi.org/10.1007/s11071-020-05875-1) contains supplementary material, which is available to authorized users.

T. Luo · M. Xu (✉)
School of Astronautics, Beihang University, Beijing 100191, China
e-mail: xuming@buaa.edu.cn

T. Luo
e-mail: luotong@buaa.edu.cn

G. Pucacco
Department of Physics, University of Roma Tor Vergata, 00133 Rome, Italy
e-mail: pucacco@roma2.infn.it

Lissajous family, are derived through the combination of the planar and the vertical Lyapunov orbits. In addition, well-known halo orbits arise at the first 1:1 bifurcation from the planar Lyapunov family [3, 4]. Halo orbits have been widely applied to many space missions thanks to their perfect locations. For example, communications satellites have been placed in a halo orbit around the translunar L_2 point [5, 6] and the International Sun–Earth Explorer-3 was placed into a halo orbit around the interior Sun–Earth L_1 point [7, 8].

The dynamics of the restricted three-body problem are significantly perturbed by nonlinear terms, which affect the stability of the linear periodic motions. Up to now, many methods have been developed to calculate and analyze the periodic motions under the effect of nonlinear terms. Lindstedt–Poincaré method is a classical approach to derive semianalytical solutions of invariant tori in SCR3BP [9–11]. Qian et al. [12] and Almeida et al. [13] studied periodic motions around an equilibrium point in the planar circular restricted three-body problem and SCR3BP within extra perturbations, respectively. Many numerical methods were proposed to generate more accurate solutions. The well-known differential correction method can be used to produce initial conditions belonging to a periodic orbit by incorporating the analytical approximations as the first guess in an iterative process [14–17]. In addition, multiple shooting method [18, 19] and multiple Poincaré sections [20] were employed to find quasiperiodic orbits in SCR3BP.

Above-mentioned methods cannot provide a deeper insight into the nature of global behavior in a neighborhood of these solutions. To give a comprehensive description of the dynamics around these collinear points, a perturbation theory based on the Lie series method [11, 21–23] is a satisfactory option. It succeeds in separating the hyperbolic and elliptic directions by constructing a normal form to perform the center manifold reduction. Combining the reduction to center manifold and a Fourier series correction method, Gomez and Mondelo [24] developed a procedure for the refinement and continuation of invariant tori. As for halo orbits, because the unperturbed linear dynamics on the two-dimensional center manifold is characterized by almost equal values of the frequencies for all mass ratios, Celletti et al. [25] and Ceccaroni et al. [26] preformed 1:1 resonant perturbation theory to investigate the halo family and to determine analytic expressions of the value of the energy at which the bifurcation takes place.

Former scholars generally focused on a specific case of SCR3BP, namely the value of the mass ratio is fixed, but the mass ratio is considered as a variable in this study. Analytical expressions of complete and resonant normal forms are derived in Sect. 2.2, and then the bifurcation energy of halo orbit is obtained as a function of mass ratio. The primary contribution of this paper is obtaining universal analytical results of Lissajous and halo orbits in SCR3BP of an arbitrary value of mass ratio. The explicit expressions of coefficients parameterized by mass ratio in these results are provided in Sect. 3 so that readers can directly extract the corresponding solutions for their interested cases. In addition, we compare the normalization method with Lindstedt–Poincaré method in Sect. 4, which confirms the rightness and effectiveness of the normalization method.

2 Reduction to center manifold

2.1 Dynamical model

To describe the motion of the small body in SCR3BP more simple, a synodic reference system (O, X, Y, Z) rotating with the angular velocity of the primaries is proposed and the units of mass, length and time are normalized so that the total mass, the distance between two primaries and the period of the motion of the primaries are 1, 1 and 2π, respectively. As shown in Fig. 1, the origin O is located at the barycenter of the primaries, the X-axis points to the larger primary from

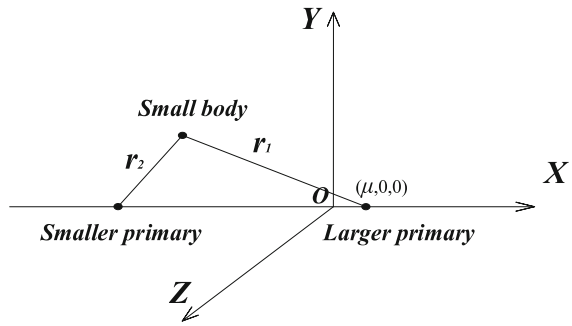

Fig. 1 The location of two primaries in the synodic reference system

the smaller one, the Z-axis is perpendicular to the motion plane of two primaries and the Y-axis is determined by right-hand rule. After the normalization, the position of the smaller primary is at $(-1+\mu, 0, 0)$, while the larger primary is at $(\mu, 0, 0)$.

The dynamical model of the small body in the synodic reference system can be expressed as

$$\ddot{\mathbf{R}} - 2\mathbf{J}\dot{\mathbf{R}} = \frac{\partial \Omega}{\partial \mathbf{R}}, \quad \mathbf{J} = \begin{bmatrix} 0 & 1 & 0 \\ -1 & 0 & 0 \\ 0 & 0 & 0 \end{bmatrix}, \tag{1}$$

where $\mathbf{R} = [X, Y, Z]^T$ is the position vector of the small body, $\Omega(X, Y, Z) = \frac{1}{2}(X^2 + Y^2) + \frac{1-\mu}{r_1} + \frac{\mu}{r_2}$ is the pseudo-potential function, $r_1 = \sqrt{(X-\mu)^2 + Y^2 + Z^2}$ and $r_2 = \sqrt{(X+1-\mu)^2 + Y^2 + Z^2}$ are the distance to two primaries, respectively. Equation (1) admits five equilibrium points, of which three points located on the X-axis are called collinear points. The origin can be moved to L_1 or L_2 point through following transformation:

$$X = -\gamma_j x + \mu + \alpha, \quad Y = -\gamma_j y, \quad Z = \gamma_j z, \tag{2}$$

where γ_j denotes the distance between L_j and the smaller primary, $\alpha = -1 + \gamma_1$ for L_1 and $\alpha = -1 - \gamma_2$ for L_2. Then, the equation of motion in the new variables can be written in the following form:

$$\begin{aligned} \ddot{x} - 2\dot{y} - (1 + 2c_2)x &= \frac{\partial}{\partial x}\sum_{n\geq 3} c_n(\mu)\rho^n P_n\left(\frac{x}{\rho}\right), \\ \ddot{y} + 2\dot{x} + (c_2 - 1)y &= \frac{\partial}{\partial y}\sum_{n\geq 3} c_n(\mu)\rho^n P_n\left(\frac{x}{\rho}\right), \\ \ddot{z} + c_2 z &= \frac{\partial}{\partial z}\sum_{n\geq 3} c_n(\mu)\rho^n P_n\left(\frac{x}{\rho}\right), \end{aligned} \tag{3}$$

where $\rho = \sqrt{x^2 + y^2 + z^2}$, p_n is the Legendre polynomials and the coefficient $c_n(\mu) = \frac{1}{\gamma_1^3}\left(\mu + (-1)^n \frac{(1-\mu)\gamma_1^{n+1}}{(1-\gamma_1)^{n+1}}\right)$ for L_1, $c_n(\mu) = \frac{(-1)^n}{\gamma_2^3}\left(\mu + \frac{(1-\mu)\gamma_2^{n+1}}{(1+\gamma_2)^{n+1}}\right)$ for L_2. By introducing the conjugated momenta $p_x = \dot{x} - y$, $p_y = \dot{y} + x$ and $p_z = \dot{z}$, the Hamiltonian function of the system can be written as

$$\begin{aligned} H = &\frac{1}{2}\left(p_x^2 + p_y^2 + p_z^2\right) + y p_x - x p_y \\ &- \sum_{n\geq 2} c_n(\mu)\rho^n P_n\left(\frac{x}{\rho}\right). \end{aligned} \tag{4}$$

The state vector at a collinear point is $[0, 0, 0, 0, 0, 0]^T$, and then the linearized Hamiltonian function about this state is

$$\begin{aligned} H_2 = &\frac{1}{2}\left(p_x^2 + p_y^2 + p_z^2\right) + y p_x - x p_y - c_2 x^2 + \frac{c_2}{2} y^2 \\ &+ \frac{c_2}{2} z^2 \end{aligned} \tag{5}$$

2.2 Normalization

Aimed at the above nearly integrable Hamiltonian system, its Hamiltonian function Eq. (4) can be simplified into specific normal form through normalization procedure. The normal form succeeds in separating the hyperbolic and elliptic behaviors so that one can study the periodic and quasiperiodic motions by only concerning the center manifolds. Reference [11] provided a detailed and clear procedures of normalization, which includes the diagonalization of quadratic part through a symplectic matrix transformation and the normalization of higher-order terms through Lie series method. Here, we do not repeat those lengthy calculations again and directly give the results.

The linearized system always has one pair of real eigenvalue, denoted by $\pm\lambda_1$, and two pairs of pure imaginary eigenvalues, denoted by $\pm\omega_1 i$ and $\pm\omega_2 i$. Then, the diagonalized form of the quadratic part can be expressed as

$$\begin{aligned} H_2(q_1, q_2, q_3, p_1, p_2, p_3) = &\lambda_1 q_1 p_1 + i\omega_1 q_2 p_2 \\ &+ i\omega_2 q_3 p_3, \end{aligned} \tag{6}$$

where $(\mathbf{q}, \mathbf{p}) = (q_1, q_2, q_3, p_1, p_2, p_3)$ are complex variables. Then, a specific normal form can be derived through a canonical transformation, which is accomplished by choosing suitable generating functions within Lie series method [11]. In complete normal form, we should preserve these monomials $\mathbf{q}^{\mathbf{k_q}}\mathbf{p}^{\mathbf{k_p}}$ (for simplicity, we have kept the same name for complex variables after normalization), where the indices satisfy

$$k_{q,1} = k_{p,1}, \quad k_{q,2} = k_{p,2}, \quad k_{q,3} = k_{p,3}. \tag{7}$$

In resonant normal form, we should preserve these monomials $\mathbf{q}^{\mathbf{k_q}}\mathbf{p}^{\mathbf{k_p}}$ where the indices satisfy

$$\begin{aligned} &k_{q,1} = k_{p,1}, \quad \left|k_{q,2} - k_{p,2}\right| = \left|k_{q,3} - k_{p,3}\right|, \\ &k_{q,2} - k_{p,2} + k_{q,3} - k_{p,3} = 0. \end{aligned} \tag{8}$$

When normalization is performed up to order 4 and the hyperbolic behaviors are removed, the complete normal form and resonant normal form of Hamiltonian function expressed by action-angle variables are

$$\begin{aligned} H^{(l,4)} = {} & \omega_1 I_{ly} + \omega_2 I_{lz} + \alpha_{2200} I_{ly}^2 + \alpha_{0022} I_{lz}^2 \\ & + \alpha_{1111} I_{ly} I_{lz}, \end{aligned} \tag{9}$$

and

$$\begin{aligned} H^{(h,4)} = {} & \omega_1 I_{hy} + \omega_2 I_{hz} + \alpha_{2200} I_{hy}^2 + \alpha_{0022} I_{hz}^2 \\ & + I_{hy} I_{hz} \left(\alpha_{1111} + 2\alpha_{2002} \cos\left(2\left(\theta_{hy} - \theta_{hz}\right)\right)\right), \end{aligned} \tag{10}$$

where ω_1, ω_2, α_{2200}, α_{0022}, α_{1111} and α_{2002} are coefficients depending only on parameter μ. The numbers of the subscript in α denote the exponents of q_2, q_3, p_2, p_3 in monomials $\mathbf{q}^{\mathbf{k_q}}\mathbf{p}^{\mathbf{k_p}}$ successively. We can distinguish that the difference between the complete normal form Eq. (9) and the resonant normal form Eq. (10) is the synchronous resonance term related to $\theta_{hy} - \theta_{hz}$, while other corresponding coefficients are completely the same. The explicit expressions of these coefficients are all listed in Appendix.

If either I_y or I_z vanishes, one obtains the nonlinear normal mode $E_y = \omega_1 I_{hy} + \alpha_{2200} I_{hy}^2$ or $E_z = \omega_2 I_{hz} + \alpha_{0022} I_{hz}^2$. For the motion in y-direction, ω_1 is the fundamental frequency and α_{2200} can be considered as a second-order coefficient for the high-order supplemented frequency. Similarly, for the motion in z-direction, ω_2 is the fundamental frequency and α_{0022} can be considered as a second-order coefficient for the high-order supplemented frequency. When I_y and I_z both exist, the motions in y- and z-direction are coupled with each other. Then, α_{1111} and α_{2002} can be considered as two coupling coefficients, which can affect the frequency in y- or z-direction through the action in the other direction. Figure 2 demonstrates the evolution of these coefficients as functions of the mass ratio, where two black lines refer to mass ratios corresponding to Sun–Earth system and Earth–Moon system, respectively. Two subgraphs in the top row correspond to ω_1 and ω_2, and two subgraphs in the bottom row correspond to α_{2200}, α_{0022}, α_{1111} and α_{2002}. The list of subgraphs on the left is the evolution of the coefficients for L_1 point, while the list of subgraphs on the right is the evolution of the coefficients for L_2 point. Two fundamental frequencies ω_1 and ω_2 correspond to the linearized motions in x–y plane and z-axis directions, respectively, and they dominate in the actual values of two motion frequencies. Subgraphs $\mathbf{a_1}$ and $\mathbf{a_2}$ demonstrate that the values of ω_1 and ω_2 always keep close, which indicates that a 1:1 resonant periodic orbit, namely the well-known halo orbit, could occur in all SCR3BP of any mass ratio. In addition, the curves are remarkably flat when the mass ratio is near or smaller than Sun–Earth system, which demonstrates that the value of motion frequencies is hardly changed with mass ratio. However, the value of motion frequencies becomes dependent on mass ratio when mass ratio is near or larger than Earth–Moon system.

2.3 Bifurcation of halo orbits

Let us implement the change in variables $\varepsilon = I_{hy} + I_{hz}$, $\Re = I_{hy}$, $\upsilon = \theta_{hz}$ and $\psi = \theta_{hy} - \theta_{hz}$. Then, Hamiltonian (10) is transformed into $H^{(tr,4)} = \omega_2\varepsilon + \delta\Re + a\Re^2 + b\varepsilon^2 + c\varepsilon\Re + d(\Re^2 - \varepsilon\Re)\cos(2\psi)$, where $\delta = \omega_1 - \omega_2$ is defined as the detuning, which provides a measure of the distance in the frequency from the synchronous resonant, and constants are $a = \alpha_{2200} + \alpha_{0022} - \alpha_{1111}$, $b = \alpha_{0022}$, $c = \alpha_{1111} - 2\alpha_{0022}$, $d = -2\alpha_{2002}$. Dynamical equations associated with $H^{(tr,4)}$ become

$$\begin{aligned} &\dot{\varepsilon} = 0, \quad \dot{\Re} = 2d\Re(\Re - \varepsilon)\sin(2\psi), \\ &\dot{\upsilon} = \omega_2 + 2b\varepsilon + c\Re - d\Re\cos(2\psi), \\ &\dot{\psi} = \delta + 2a\Re + c\varepsilon + d(2\Re - \varepsilon)\cos(2\psi). \end{aligned} \tag{11}$$

When the value of ε is fixed, we obtain a one-degree-of-freedom system in the phase plane $(\Re, \psi)$. Its equilibria correspond to periodic orbits of the original system. If $\Re = \varepsilon$, then the motion takes place in x–y plane, which approximately corresponds to the planar Lyapunov orbit. If $\psi = \pm\pi/2$, the equilibrium points $(\Re_l, \pm\pi/2)$ correspond to loop orbits. By solving $\dot{\psi} = 0$, we can obtain $\Re_l = -\frac{\delta + (c+d)\varepsilon}{2(a-d)}$. Halo orbits are these loop orbits bifurcating from the planar Lyapunov orbit. Thus, the quantity ε_{ly} marking the occurrence of the bifurcation of the halo orbits can be

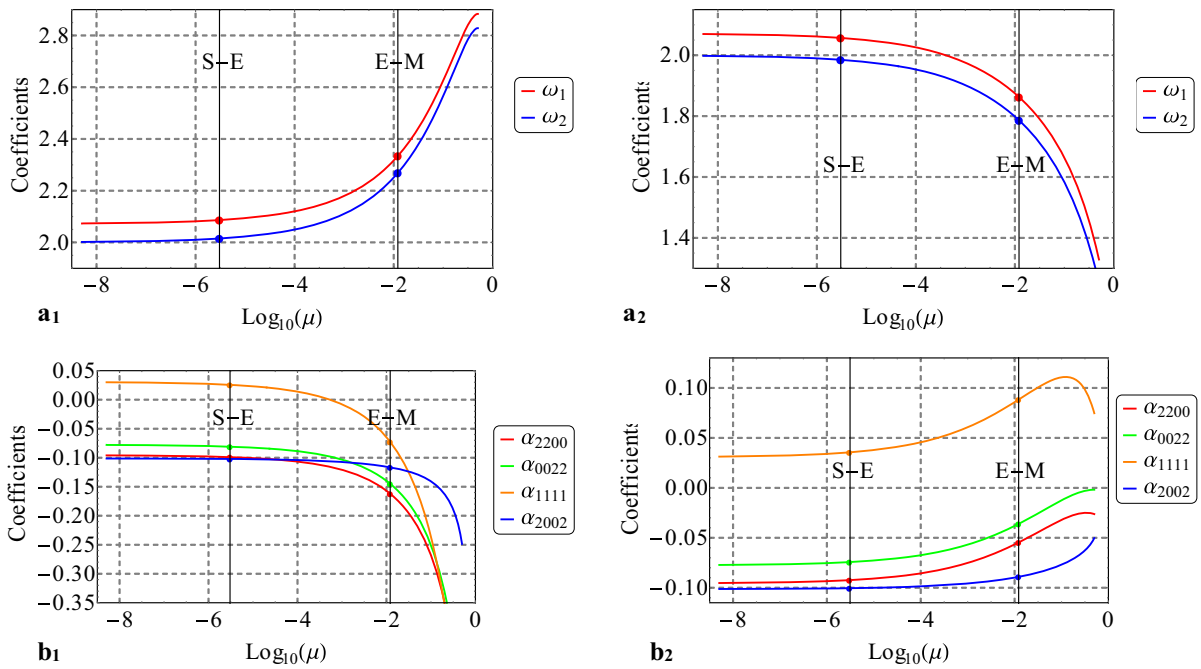

Fig. 2 Coefficients in Eq. (10) as functions of the mass ratio: $\mathbf{a_1}$ and $\mathbf{b_1}$ are the evolution of the coefficients for L_1 point; $\mathbf{a_2}$ and $\mathbf{b_2}$ are the evolution of the coefficients for L_2 point

solved from $\Re_l = \varepsilon$ and the solution is $\varepsilon_{ly} = -\frac{\delta}{2a+c-d}$. The energy level at which a bifurcation to halo orbit occurs can be estimated as $E = \omega_2 \varepsilon_{ly}$, which, coming back to the original coefficients, gives the bifurcation value

$$E = \frac{\omega_2(\omega_1 - \omega_2)}{\alpha_{1111} - 2(\alpha_{2200} - \alpha_{2002})}. \tag{12}$$

Figure 3 shows the bifurcation thresholds computed via Eq. (12) as a function of the mass ratio, where the red and blue lines correspond to L_1 and L_2 points, respectively, and two black lines referring to mass ratios correspond to the Sun–Earth system and Earth–Moon system, respectively. The procedure of the bifurcation of halo orbit can be described by Poincaré section method. Figures 4 and 5 provide the evolution of dynamics around L_1 point in the Earth–Moon system and Sun–Earth system, respectively. Bifurcation thresholds in two systems are located within the ranges of [0.3, 0.33] and [0.33, 0.35], respectively, which matches the analytical results in Fig. 3.

3 Analytical solutions of halo and Lissajous orbits

3.1 Lissajous orbits

The inverse transformation of complete normal form derives the analytical solutions of Lissajous orbits. When the complete normalization is implemented up to order 4, the explicit expressions of the initial position variables as functions of the final action-angle variables can be written as

$$\begin{aligned}
X_l &= X_{l1} + X_{l2} + X_{l3} + \cdots,\\
X_{l1} &= X\beta_{0100}\sqrt{I_y}\cos\theta_y,\\
X_{l2} &= X\beta_{2000} I_y \sin^2\theta_y + X\beta_{0200} I_y \cos^2\theta_y\\
&\quad + X\beta_{0020} I_z \sin^2\theta_z + X\beta_{0002} I_z \cos^2\theta_z,\\
X_{l3} &= X\beta_{2100}\sqrt{I_y^3}\sin^2\theta_y\cos\theta_y\\
&\quad + X\beta_{1011}\sqrt{I_y} I_z \sin\theta_y\cos\theta_y\cos\theta_z + X\beta_{0300}\sqrt{I_y^3}\cos^3\theta_y\\
&\quad + X\beta_{0120}\sqrt{I_y} I_z \cos\theta_y\sin^2\theta_z + X\beta_{0102}\sqrt{I_y} I_z \cos\theta_y\cos^2\theta_z;
\end{aligned} \tag{13}$$

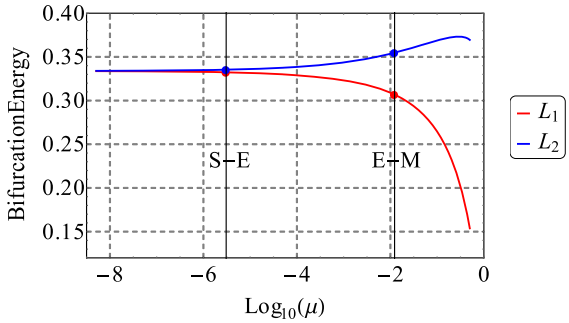

Fig. 3 Bifurcation thresholds computed via Eq. (12) as a function of the mass ratio: the red line for L_1 and the blue line for L_2

$$
\begin{aligned}
Y_l &= Y_{l1} + Y_{l2} + Y_{l3} + \cdots,\\
Y_{l1} &= Y\beta_{1000}\sqrt{I_y}\sin\theta_y,\\
Y_{l2} &= Y\beta_{1100} I_y \sin\theta_y \cos\theta_y + Y\beta_{0011} I_z \sin\theta_z \cos\theta_z,\\
Y_{l3} &= Y\beta_{3000}\sqrt{I_y^3}\sin^3\theta_y + Y\beta_{1200}\sqrt{I_y^3}\sin\theta_y\cos^2\theta_y\\
&\quad + Y\beta_{1020}\sqrt{I_y} I_z \sin\theta_y \sin^2\theta_z\\
&\quad + Y\beta_{1002}\sqrt{I_y} I_z \sin\theta_y \cos^2\theta_z\\
&\quad + Y\beta_{0111}\sqrt{I_y} I_z \cos\theta_y \sin\theta_z \cos\theta_z;
\end{aligned}
\tag{14}
$$

$$
\begin{aligned}
Z_l &= Z_{l1} + Z_{l2} + Z_{l3} + \cdots,\\
Z_{l1} &= Z\beta_{0010}\sqrt{I_z}\sin\theta_z,\\
Z_{l2} &= Z\beta_{1001}\sqrt{I_y}\sqrt{I_z}\sin\theta_y\cos\theta_z + Z\beta_{0110}\sqrt{I_y}\sqrt{I_z}\cos\theta_y\sin\theta_z,\\
Z_{l3} &= Z\beta_{2010} I_y\sqrt{I_z}\sin^2\theta_y\sin\theta_z + Z\beta_{1101} I_y\sqrt{I_z}\sin\theta_y\cos\theta_y\cos\theta_z\\
&\quad + Z\beta_{0210} I_y\sqrt{I_z}\cos^2\theta_y\sin\theta_z\\
&\quad + Z\beta_{0030}\sqrt{I_z^3}\sin^3\theta_z + Z\beta_{0012}\sqrt{I_z^3}\sin\theta_z\cos^2\theta_z;
\end{aligned}
\tag{15}
$$

where X_{l1}, Y_{l1} and Z_{l1}, X_{l2}, Y_{l2} and Z_{l2}, and X_{l3}, Y_{l3} and Z_{l3} are, respectively, defined as the first-order, second-order and third-order terms of position variables, and $X\beta_{0100}$, $X\beta_{2000}$, …, and $Z\beta_{0012}$ (see "Online Appendix" for explicit expressions) are coefficients which only depend on the mass ratio of the system. The four numbers in the subscripts of $X\beta_{0100}$, $X\beta_{2000}$, …, and $Z\beta_{0012}$ successively correspond to the indexes of $\sin\theta_y$, $\cos\theta_y$, $\sin\theta_z$ and $\cos\theta_z$. As we can see, every term is constructed based on the triangular series of θ_y and θ_z, which determines the quasiperiodic change of these position variables. The explicit expressions of $X\beta_{0100}$, $X\beta_{2000}$, …, and $Z\beta_{0012}$ are listed in the "Online Appendix." Figures 6 and 7 show the evolutions of coefficients in the analytical solution of Lissajous orbits around L_1 point and L_2 point, respectively. The first, second and third rows correspond to coefficients in Eqs. (13), (14) and (15), respectively. Similar to the changing tendencies of motion frequencies in Fig. 2, these coefficients vary slowly when the mass ratio is near or smaller than Sun–Earth system, while coefficients vary drastically when the mass ratio is near or larger than Earth–Moon system.

3.2 Halo orbits

The inverse transformation of resonant normal form derives the analytical solutions of halo orbits. When the resonant normalization form is implemented up to order 4, the explicit expressions of the initial position variables as functions of the final action-angle variables can be written as

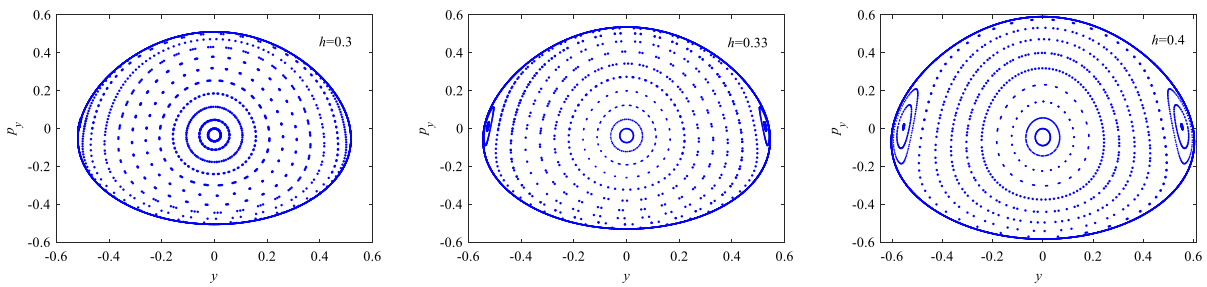

Fig. 4 Bifurcation of halo orbit around L_1 point in the Earth–Moon system

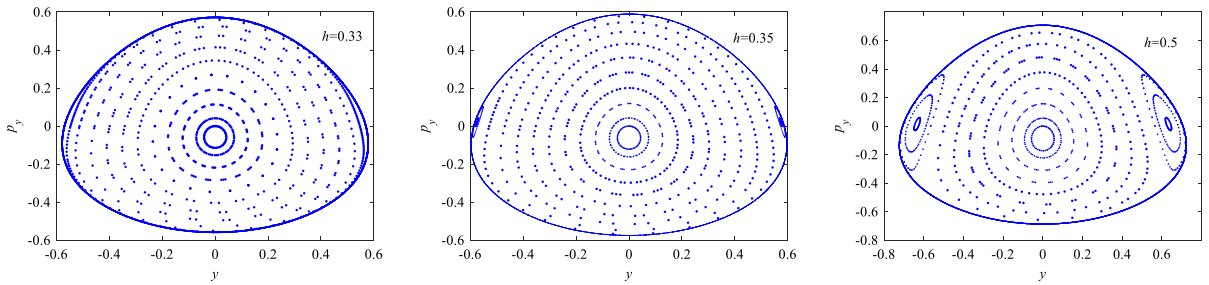

Fig. 5 Bifurcation of halo orbit around L_1 point in the Sun–Earth system

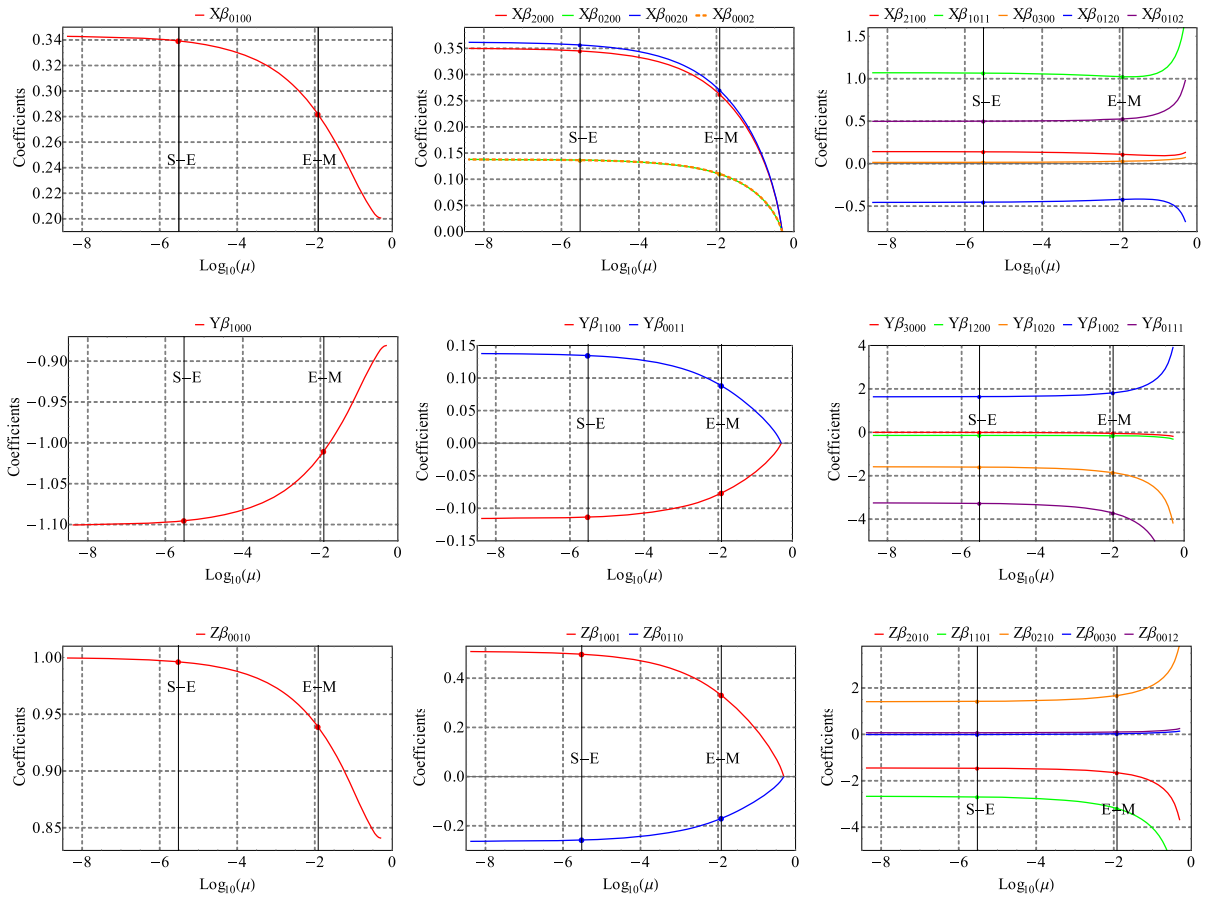

Fig. 6 Coefficients in the analytical solution of Lissajous orbits around L_1 point: the first, second and third rows are for X, Y, and Z

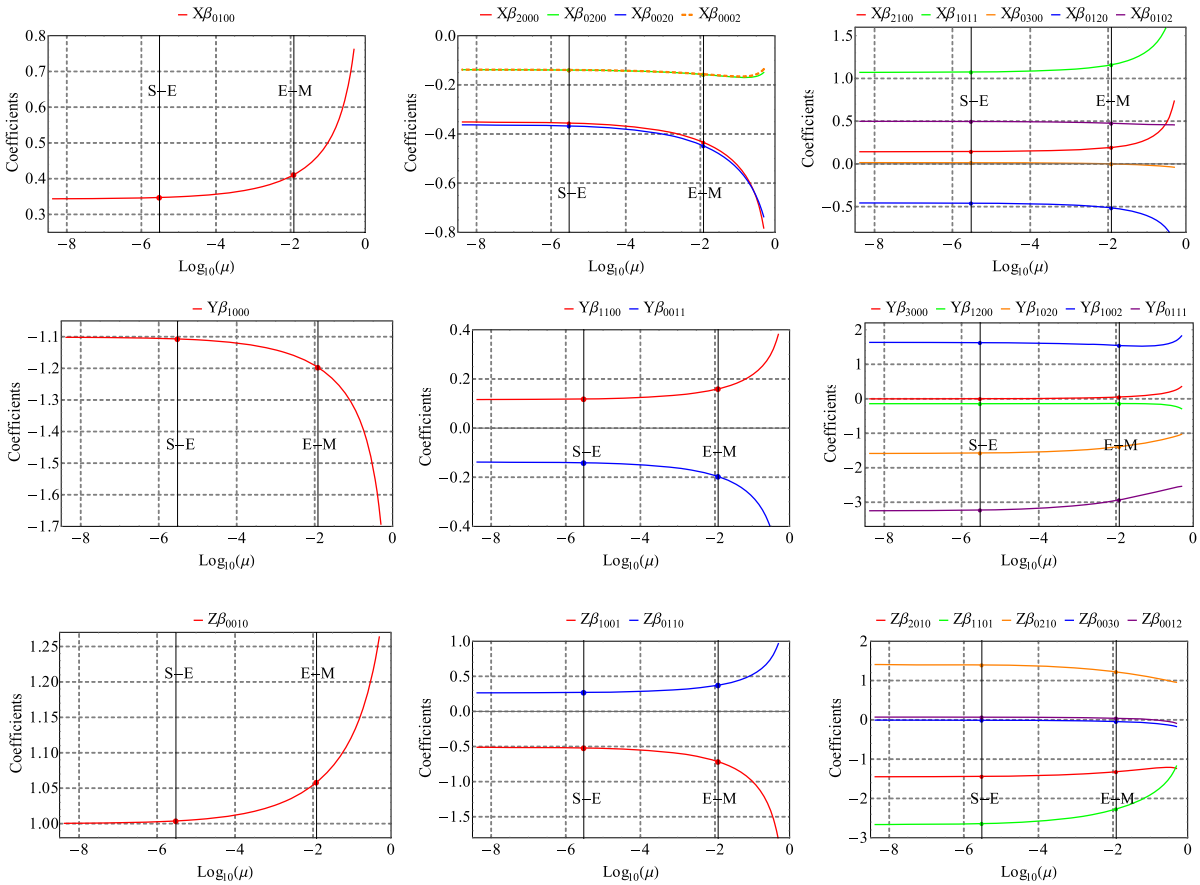

Fig. 7 Coefficients in the analytical solution of Lissajous orbits around L_2 point: the first, second and third rows are for X, Y, and Z

$$
\begin{aligned}
X_h &= X_{h1} + X_{h2} + X_{h3} + \cdots,\\
X_{h1} &= X\gamma_{10}^{01}\sqrt{I_y}\cos\theta_y,\\
X_{h2} &= X\gamma_{20}^{20} I_y \sin^2\theta_y + X\gamma_{02}^{20} I_z \sin^2\theta_y\\
&\quad + X\gamma_{20}^{02} I_y \cos^2\theta_y + X\gamma_{02}^{02} I_z \cos^2\theta_y,\\
X_{h3} &= X\gamma_{30}^{21}\sqrt{I_y^3}\sin^2\theta_y\cos\theta_y\\
&\quad + X\gamma_{12}^{21}\sqrt{I_y} I_z \sin^2\theta_y\cos\theta_y\\
&\quad + X\gamma_{30}^{03}\sqrt{I_y^3}\cos^3\theta_y + X\gamma_{12}^{03}\sqrt{I_y} I_z \cos^3\theta_y;
\end{aligned}
\tag{16}
$$

$$
\begin{aligned}
Y_h &= Y_{h1} + Y_{h2} + Y_{h3} + \cdots,\\
Y_{h1} &= Y\gamma_{10}^{10}\sqrt{I_y}\sin\theta_y,\\
Y_{h2} &= Y\gamma_{20}^{11} I_y \sin\theta_y\cos\theta_y + Y\gamma_{02}^{11} I_z \sin\theta_y\cos\theta_y,\\
Y_{h3} &= Y\gamma_{30}^{30}\sqrt{I_y^3}\sin^3\theta_y + Y\gamma_{12}^{30}\sqrt{I_y} I_z \sin^3\theta_y\\
&\quad + Y\gamma_{30}^{12}\sqrt{I_y^3}\sin\theta_y\cos^2\theta_y + Y\gamma_{12}^{12}\sqrt{I_y} I_z \sin\theta_y\cos^2\theta_y;
\end{aligned}
\tag{17}
$$

$$
\begin{aligned}
Z_h &= Z_{h1} + Z_{h2} + Z_{h3} + \cdots,\\
Z_{h1} &= Z\gamma_{01}^{01}\sqrt{I_z}\cos\theta_y,\\
Z_{h2} &= Z\gamma_{11}^{20}\sqrt{I_y}\sqrt{I_z}\sin^2\theta_y + Z\gamma_{11}^{02}\sqrt{I_y}\sqrt{I_z}\cos^2\theta_y,\\
Z_{h3} &= Z\gamma_{21}^{21} I_y\sqrt{I_z}\sin^2\theta_y\cos\theta_y\\
&\quad + Z\gamma_{03}^{21}\sqrt{I_z^3}\sin^2\theta_y\cos\theta_y + Z\gamma_{21}^{03} I_y\sqrt{I_z}\cos^3\theta_y\\
&\quad + Z\gamma_{03}^{03}\sqrt{I_z^3}\cos^3\theta_y;
\end{aligned}
\tag{18}
$$

where X_{h1}, Y_{h1} and Z_{h1}, X_{h2}, Y_{h2} and Z_{h2}, and X_{h3}, Y_{h3} and Z_{h3} are, respectively, defined as the first-order, second-order and third-order terms of position variables, and $X\gamma_{10}^{01}$, $X\gamma_{20}^{20}$, …, and $Z\gamma_{03}^{03}$. (see "Online Appendix" for explicit expressions) are coefficients which only depend on the mass ratio of the system. The two numbers in the superscripts of $X\gamma_{10}^{01}$., $X\gamma_{20}^{20}$, …,

and $Z\gamma_{03}^{03}$ successively correspond to the indexes of $\sin\theta_y$ and $\cos\theta_y$, while the numbers in the subscripts of $X\gamma_{10}^{01}$., $X\gamma_{20}^{20}$, …, and $Z\gamma_{03}^{03}$ successively correspond to the indexes of $\sqrt{I_y}$ and $\sqrt{I_z}$. Different from the expressions for Lissajous orbits, every term is constructed only based on the triangular series of θ_y, which determines the periodic change in position variables. The explicit expressions of $X\gamma_{10}^{01}$, $X\gamma_{20}^{20}$, …, and $Z\gamma_{03}^{03}$ are listed in the "Online Appendix." Figures 8 and 9 show the evolutions of coefficients in the analytical solution of halo orbits around L_1 point and L_2 point, respectively. The first, second and third rows correspond to coefficients in Eqs. (16), (17) and (18), respectively. Similarly, these coefficients vary slowly when the mass ratio is near or smaller than Sun–Earth system, while coefficients vary drastically when the mass ratio is near or larger than Earth–Moon system.

4 Comparison with Lindstedt–Poincaré method

In Ref. [10], Richardson presented a third-order analytical solution for halo orbit around the collinear points of the SCR3BP through the Lindstedt–Poincaré method. The key techniques of the Lindstedt–Poincaré method are eliminating the secular terms and solving ordinary differential equations, which make it difficult to be achieved through programmatic approach on computer. In comparison, the analytical solutions can be extended to higher order by simply setting the order of normalization when we adopt the method proposed in this paper. In addition, the analytical solution for Lissajous orbit is also obtained through the normalization method, which can be considered as a great contribution of this paper. In Ref. [11], Jorba and Masdemont obtained semianalytical solutions for halo and Lissajous orbits through the Lindstedt–Poincaré

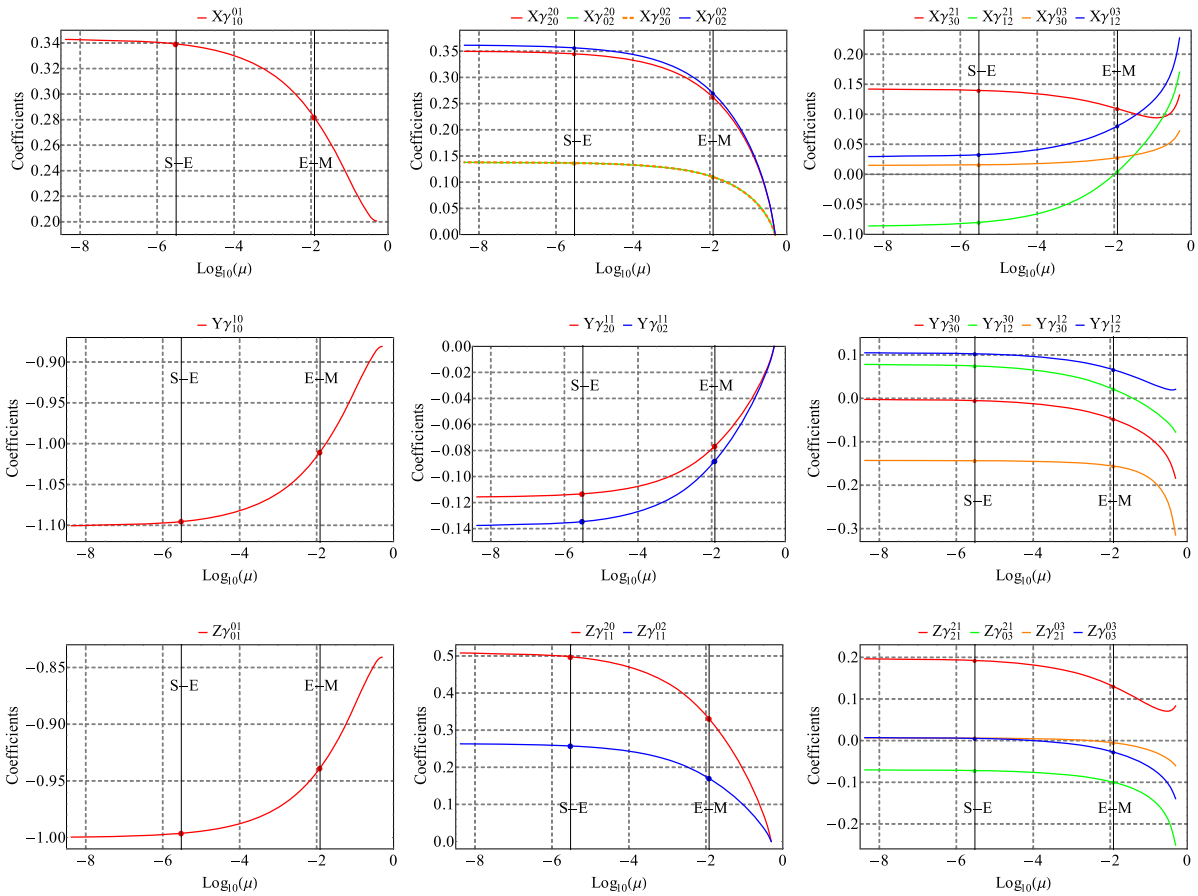

Fig. 8 Coefficients in the analytical solution of halo orbits around L_1 point: the first, second and third rows are for X, Y, and Z

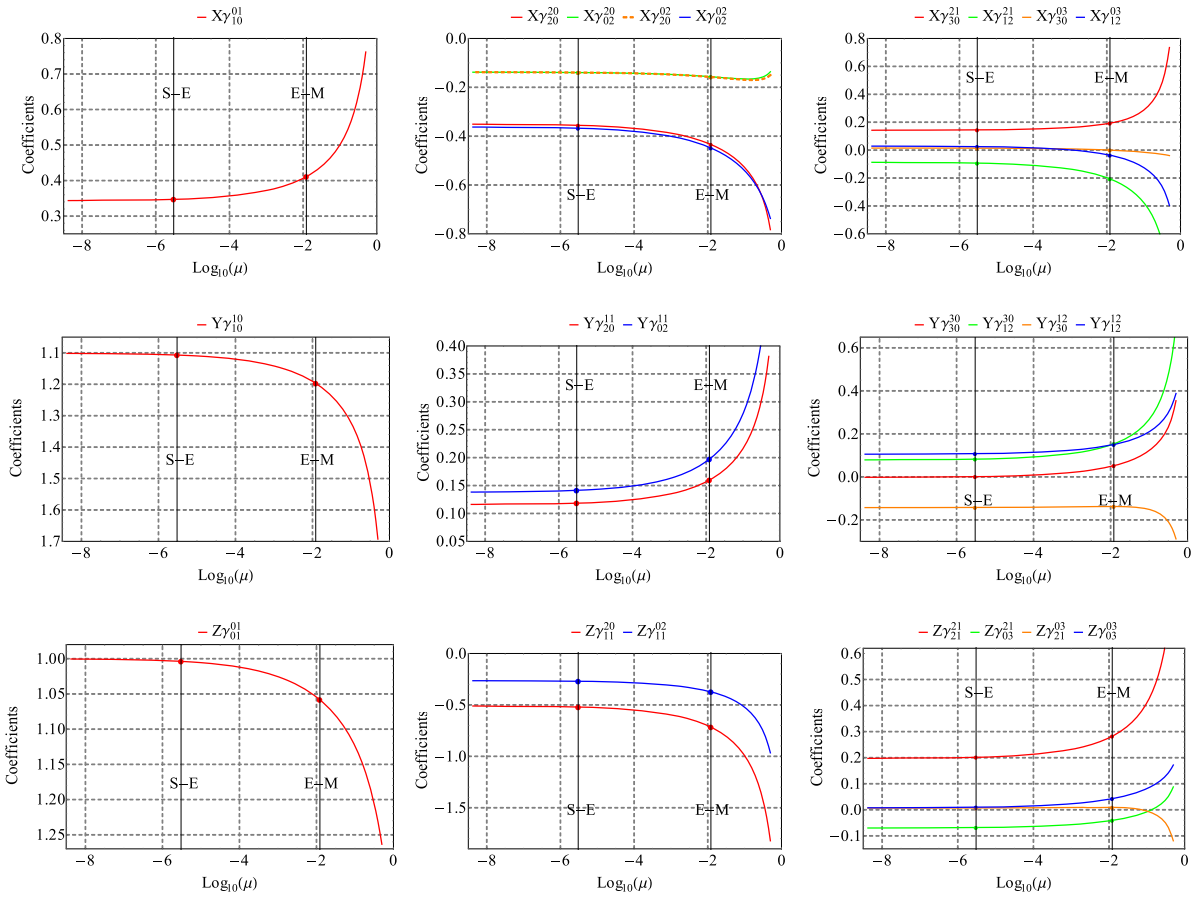

Fig. 9 Coefficients in the analytical solution of halo orbits around L_2 point: the first, second and third rows are for X, Y, and Z

method. Although they provided the results expanded as formal series in powers of the amplitudes, the coefficients in the series could not be explicitly expressed and were computed again for a particular case. In this paper, not only is the solution for Lissajous orbit expanded as series in powers of the amplitudes, but also the coefficients in the series are explicitly expressed as functions of mass ratio. Thus, the analytical solutions obtained in this paper can be directly applied to a particular case without complicated computation once again.

Delshams et al. [27] compared Lindstedt–Poincaré series with Birkhoff normal forms in the spatial Hill's problem, and they proved that the truncated Lindstedt–Poincaré series was just the solution to the truncated Birkhoff normal form equations. Here, the numerical results for halo and Lissajous orbits in the SCR3BP are calculated through Lindstedt–Poincaré method and normalization method, respectively, and then we perform a comparison between them. According to Ref. [11], the result for Lissajous orbit derived by Lindstedt–Poincaré method is

$$
\begin{aligned}
X &= \sum_{i,j=1}^{\infty} \left(\sum_{|k|\le i, |m|\le j} X_{ijkm} \cos(k\theta_1 + m\theta_2) \right) \alpha^i \beta^j, \\
Y &= \sum_{i,j=1}^{\infty} \left(\sum_{|k|\le i, |m|\le j} Y_{ijkm} \sin(k\theta_1 + m\theta_2) \right) \alpha^i \beta^j, \\
Z &= \sum_{i,j=1}^{\infty} \left(\sum_{|k|\le i, |m|\le j} Z_{ijkm} \sin(k\theta_1 + m\theta_2) \right) \alpha^i \beta^j,
\end{aligned}
\tag{19}
$$

where $\theta_1 = \omega t + \phi_1$, $\theta_2 = \upsilon t + \phi_2$, $\omega = \sum_{i,j=0}^{\infty} \omega_{ij}\alpha^i\beta^j$ and $\upsilon = \sum_{i,j=0}^{\infty} \upsilon_{ij}\alpha^i\beta^j$. To match the first order of the analytical solutions obtained in Sect. 3.1, namely Eqs. (13)–(15), we set the value of X_{1010}, Y_{1010}, Z_{0101}, ω_{00} and υ_{00} as

$$X_{1010} = X\beta_{0100}, \quad Y_{1010} = Y\beta_{1000}, \quad Z_{0101} = Z\beta_{0010}, \quad \omega_{00} = \omega_1, \ \upsilon_{00} = \omega_2. \tag{20}$$

Table 1 shows the numerical results of the coefficients of the Lissajous expansions around L_1 point in the Sun–Earth system, up to order 3. By substituting the mass ratio of the Sun–Earth system into Eqs. (13)–(15) and transforming the trigonometric series into the form of Eq. (19), we can obtain the numerical results as

$$\begin{aligned} X_l = {} & 0.33917\sqrt{I_y}\cos\theta_y + 0.24074I_y + 0.24642I_z \\ & - 0.10422I_y\cos 2\theta_y - 0.10999I_z\cos 2\theta_z \\ & + 0.04674\sqrt{I_y^3}\cos\theta_y + 0.02322\sqrt{I_y}I_z\cos\theta_y \\ & - 0.03097\sqrt{I_y^3}\cos 3\theta_y + 0.50491\sqrt{I_y}I_z\cos(\theta_y - 2\theta_z) \\ & - 0.02823\sqrt{I_y}I_z\cos(\theta_y + 2\theta_z). \end{aligned} \tag{21}$$

$$\begin{aligned} Y_l = {} & -1.09527\sqrt{I_y}\sin\theta_y - 0.05665I_y\sin 2\theta_y \\ & + 0.06725I_z\sin 2\theta_z \\ & - 0.03993\sqrt{I_y^3}\sin\theta_y + 0.02179\sqrt{I_y}I_z\sin\theta_y \\ & - 0.03456\sqrt{I_y^3}\sin 3\theta_y \\ & + 1.62985\sqrt{I_y}I_z\sin(\theta_y - 2\theta_z) \\ & - 0.00701\sqrt{I_y}I_z\sin(\theta_y + 2\theta_z). \end{aligned} \tag{22}$$

$$\begin{aligned} Z_l = {} & 0.99622\sqrt{I_z}\sin\theta_z + 0.37738\sqrt{I_y}\sqrt{I_z}\sin(\theta_y - \theta_z) \\ & + 0.11993\sqrt{I_y}\sqrt{I_z}\sin(\theta_y + \theta_z) \\ & - 0.0185I_y\sqrt{I_z}\sin\theta_z + 0.01403\sqrt{I_z^3}\sin\theta_z \\ & + 0.01931\sqrt{I_z^3}\sin 3\theta_z \\ & + 0.04654I_y\sqrt{I_z}\sin(2\theta_y + \theta_z) \\ & - 1.3942I_y\sqrt{I_z}\sin(2\theta_y - \theta_z). \end{aligned} \tag{23}$$

It turns out that the coefficients in Eq. (21)-(23) completely equal the corresponding coefficients in Table 1, which verifies that the solutions for the Lissajous orbit derived through normalization method and Lindstedt–Poincaré method are the same. This comparison result confirms the rightness and effectiveness of the normalization method.

In order to apply the Lindstedt–Poincaré method to solving halo orbit, we must modify Eq. (3) by adding the product of the factors $\triangle$ and z to the third equation, namely $\ddot{z} + c_2 z = \frac{\partial}{\partial z}\sum_{n\geq 3} c_n(\mu)\rho^n P_n\left(\frac{x}{\rho}\right) + \Delta z$, where the factor $\triangle$ is expanded as a frequency-type series $\Delta = \sum_{i,j=0}^{\infty} d_{ij}\alpha^i\beta^j$, with the condition $\triangle = 0$. To make sure periodic motions appear in the linearized equation, the value of d_{00} is set as $d_{00} = \omega_2^2 - \omega_1^2$. Then, the result for halo orbit can be expressed as

$$\begin{aligned} X &= \sum_{i,j=1}^{\infty}\left(\sum_{|k|\leq i+j} X_{ijk}\cos(k\theta)\right)\alpha^i\beta^j, \\ Y &= \sum_{i,j=1}^{\infty}\left(\sum_{|k|\leq i+j} Y_{ijk}\sin(k\theta)\right)\alpha^i\beta^j, \\ Z &= \sum_{i,j=1}^{\infty}\left(\sum_{|k|\leq i+j} Z_{ijk}\cos(k\theta)\right)\alpha^i\beta^j, \end{aligned} \tag{24}$$

where $\theta = \omega t + \phi$ and $\omega = \sum_{i,j=0}^{\infty}\omega_{ij}\alpha^i\beta^j$. To match the first order of the analytical solution obtained in Sect. 3.2, namely Eqs. (16)–(18), we set the value of X_{101}, Y_{101}, Z_{011} and ω_{00} as

$$X_{101} = X\gamma_{10}^{01}, \quad Y_{101} = Y\gamma_{10}^{10}, \quad Z_{011} = Z\gamma_{01}^{01}, \quad \omega_{00} = \omega_1. \tag{25}$$

Table 2 shows the numerical results of the coefficients of the halo expansions around L_1 point in the Sun–Earth system, up to order 3. By substituting the mass ratio of the Sun–Earth system into Eqs. (16)–(18) and transforming the trigonometric series into the form of Eq. (24), we can obtain the numerical results as

Table 1 Coefficients, up to order 3 of the Lindstedt–Poincaré expansion of the Lissajous orbits around L_1 in the Sun–Earth system

i	j	ω_{ij}	υ_{ij}
0	0	.2086453564223108E+01	.2015210662996640E+01
2	0	− .19793330921103466E+00	.25623574529952564E−01
0	2	.25623574529952564E−01	.16195976981230506E+00

i	j	k	m	X_{ijkm} or Z_{ijkm}	Y_{ijkm}
1	0	1	0	.3391700424065888E+00	− .1095270999402855E+01
0	1	0	1	.9962189144672732E+00	
2	0	0	0	.240735994312677E+00	.0000000000000000E+00
2	0	2	0	− .10421885417013624E+00	− .5664916013778637E−01
0	2	0	0	.24642355008239508E+00	.0000000000000000E+00
0	2	0	2	− 10998869627427148E+00	.6725227040176095E−01
1	1	1	− 1	.3773759739986624E+00	
1	1	1	1	.11993162155276677E+00	
3	0	1	0	.46739047397258086E−01	− .3992674505450506E−01
3	0	3	0	− .30972381614462682E−01	− .3455727466578585E−01
1	2	1	− 2	.5049132658541867E+00	.1629854700400192E+01
1	2	1	0	.2322490685452064E−01	.2179380433454126E−01
1	2	1	2	− .2823410205572303E−01	− .701118576211499E−02
2	1	2	− 1	− .1394200550803349E+01	
2	1	2	1	.4653723699886294E−01	
0	3	0	3	.1930655501929184E−01	

$$
\begin{aligned}
X_h = {} & 0.33917\sqrt{I_y}\cos\theta_y + 0.24074 I_y + 0.24642 I_z \\
& - 0.10422 I_y \cos 2\theta_y - 0.10999 I_z \cos 2\theta_y \\
& + 0.04674\sqrt{I_y^3}\cos\theta_y + 0.05146\sqrt{I_y} I_z \cos\theta_y \\
& - 0.03097\sqrt{I_y^3}\cos 3\theta_y - 0.01866\sqrt{I_y} I_z \cos 3\theta_y,
\end{aligned} \tag{26}
$$

$$
\begin{aligned}
Y_h = {} & -1.09527\sqrt{I_y}\sin\theta_y - 0.05665 I_y \sin 2\theta_y \\
& + 0.06725 I_z \sin 2\theta_y - 0.03993\sqrt{I_y^3}\sin\theta_y \\
& + 0.01478\sqrt{I_y} I_z \sin\theta_y - 0.03456\sqrt{I_y^3}\sin 3\theta_y \\
& - 0.05961\sqrt{I_y} I_z \sin 3\theta_y,
\end{aligned} \tag{27}
$$

$$
\begin{aligned}
Z_h = {} & -0.99622\sqrt{I_z}\cos\theta_y - 0.11993\sqrt{I_y}\sqrt{I_z} \\
& + 0.37738\sqrt{I_y}\sqrt{I_z}\cos 2\theta_y \\
& - 0.02804 I_y\sqrt{I_z}\cos\theta_y - 0.01403\sqrt{I_z^3}\cos\theta_y \\
& + 0.03404 I_y\sqrt{I_z}\cos 3\theta_y + 0.01931\sqrt{I_z^3}\cos 3\theta_y,
\end{aligned} \tag{28}
$$

It turns out that some coefficients in Eq. (26)–(28) equal the corresponding coefficients in Table 2, while others are different. Moreover, in order to compare the analytical solutions derived through these two methods, we reset the linearized solution in Lindstedt–Poincaré procedure, namely Eqs. (4a)–(4c) in Ref. [11], as

$$
\begin{aligned}
& X = X\gamma_{10}^{01}\alpha\cos\theta, \quad Y = Y\gamma_{10}^{10}\alpha\sin\theta, \\
& Z = Z\gamma_{01}^{01}\beta\cos\theta.
\end{aligned} \tag{29}
$$

Then, following the Lindstedt–Poincaré procedure, we can also derive a third-order analytical solution for halo orbit. Here, we do not give the complicated expressions anymore. Results demonstrate that those coefficients whose numerical solutions are equal in two methods also have the same analytical expressions, while those coefficients whose numerical solutions are different in two methods also have the different analytical expressions. In summary, we can obtain the same conclusion that the solutions for halo orbits derived by these two methods are partly different through comparing analytical or numerical solutions. The reason causing the differences is that

Table 2 Coefficients, up to order 3 of the Lindstedt–Poincaré expansion of the halo orbits around L_1 in the Sun–Earth system

i	j		ω_{ij}	d_{ij}
0	0		.2086453564223108E+01	− .2922144544766949E+00
2	0		− .1979330921103466E+00	.1836623714737889E+01
0	2		.2507595139106262 3E+00	− .1727760457991 7996E+01
i	j	k	X_{ijk} or Z_{ijk}	Y_{ijk}
1	0	1	.3391700424065888E+00	− .1095270999402855E+01
0	1	0	− .9962189144672732E+00	
2	0	0	.240735994312677E+00	.0000000000000000E+00
2	0	2	− .10421885417013624E+00	− .5664916013778637E−01
0	2	0	.24642355008239508E+00	.0000000000000000E+00
0	2	2	.10367563403440155E+00	− .60287960157057424E−01
1	1	0	.3516046249740591E+00	
1	1	2	− .11720154165801971E+00	
3	0	1	.0000000000000000E+00	.11100616986539415E+00
3	0	3	− .30972381614462682E−01	− .3455727466578585E−01
1	2	1	.0000000000000000E+00	.1453120544073662E+00
1	2	3	.2783272992989514E−01	.7748704911540644E−02
2	1	3	.4562227542349283E−01	
0	3	3	.18828666341107515E−01	

the dynamical equation is modified during the Lindstedt–Poincaré procedure, but maintained as the original form during normalization method.

Because of the differences, it is necessary to compare the accuracy of the halo orbits derived through these two methods. Here, we consider a numerical solution generated by differential correction method is accurate, and then use $\sqrt{\delta X^2 + \delta Y^2 + \delta Z^2}$ (δX, δY and δZ are the errors between two trajectories along X-axis, Y-axis and Z-axis, respectively) to estimate the error between a third-order analytical solution and the corresponding numerical solution. For normalization method, we choose $I_y = 0.3040, I_z = 0.1501, \theta_y = 0$, and the initial state is determined as $\mathbf{A}_0 = [-0.989011, 0, 0.004404, 0, -0.011665, 0]^T$. For Lindstedt–Poincaré method, we choose $\alpha = 0.1870$, $\beta = 0.3909$, $\theta = 0$, and the initial state is determined as $\mathbf{A}_0 = [-0.989097, 0, 0.004465, 0, -0.011705, 0]^T$. Figure 10 gives the varying curve of the error during one period of the halo orbit, where the blue line corresponds to normalization method and the red line corresponds to Lindstedt–Poincaré method. As we can see, two curves have the same changing rules: There exist twice oscillations during one period, and the moments of occurrence of two peaks and one trough are close as well. The magnitudes of two errors are both 10^{-4}, which indicates that the accuracies of the halo orbits derived

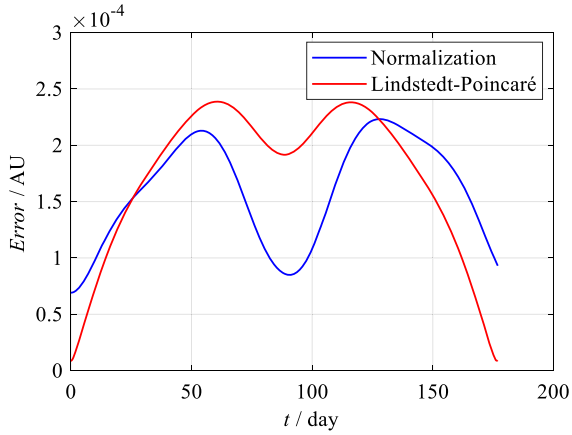

Fig. 10 Errors between the analytical and numerical solutions for normalization method and Lindstedt–Poincaré method

through the normalization method and Lindstedt–Poincaré method can be considered roughly the same. In addition, the maximum value and variation range of the error for the normalization method are both less than those of the error for Lindstedt–Poincaré method. Thus, from this viewpoint, the analytical solutions derived by the normalization method are better.

5 Conclusions

Aimed at collinear points L_1 and L_2 in a spatial circular restricted three-body problem of an arbitrary value of the mass ratio, we succeed in obtaining the analytical forms of complete and resonant normalized Hamiltonian functions. The expressions of the coefficients in the normalization forms are explicitly provided as functions of the mass ratio, and the formula for the energy threshold at which the bifurcation to halo orbits occurs is derived. Through implementing the inverse process of complete and resonant normalization, we can, respectively, generate the universal analytical solutions of Lissajous and halo orbits in the initial synodic reference system, which is considered as a great contribution of this paper. In the explicit third-order analytical solutions of Lissajous and halo orbits, three position variables are both expressed as series forms of normalized action and angle variables and the coefficients are both parameterized by the mass ratio. According to comparison results, the third-order analytical solutions of Lissajous orbits derived through normalization method and Lindstedt–Poincaré method are completely the same, which indicates the validity and feasibility of the proposed normalization method. The solutions of halo orbits derived through two methods are different, but the maximum value and variation range of the error for the normalization method are both less than those of the error for Lindstedt–Poincaré method.

Acknowledgements This study was funded by the National Natural Science Foundation of China (11772024 and 11432001), the Fundamental Research Funds for the Central Universities and the Foundation of Key Laboratory of Spacecraft Design Optimization and Dynamic Simulation Technologies, Ministry of Education of China.

Compliance with ethical standards

Conflict of interest The authors declare that they have no conflict of interest.

Appendix: Coefficients in two normal forms

Complete normal form: $H^{(CM,4)} = \omega_1 I_{ly} + \omega_2 I_{lz} + \alpha_{2200} I_{ly}^2 + \alpha_{0022} I_{lz}^2 + \alpha_{1111} I_{ly} I_{lz}$.

Resonant normal form: $H^{(CM,4)} = \omega_1 I_{hy} + \omega_2 I_{hz} + \alpha_{2200} I_{hy}^2 + \alpha_{0022} I_{hz}^2 + I_{hy} I_{hz} (\alpha_{1111} + 2\alpha_{2002} \cos(2(\theta_{hy} - \theta_{hz})))$.

The coefficients are listed as follows.

$$\omega_1 = \frac{\sqrt{2 - c_2 + \sqrt{c_2 \sqrt{-8 + 9c_2}}}}{\sqrt{2}}$$

$$\omega_2 = \sqrt{c_2}$$

$$\alpha_{2200} = \frac{3\left(\begin{array}{r}\left(\begin{array}{r}1120 - 8944c_2 + 17376c_2^2 - 11100c_2^3 + 2025c_2^4 + 3402c_2^5\\ +\left(1776c_2^{1/2} - 3368c_2^{3/2} + 4616c_2^{5/2} + 1179c_2^{7/2} + 1134c_2^{9/2}\right)t_1\end{array}\right)c_3^2\\ -3(1+2c_2)\left(\begin{array}{r}96 - 1072c_2 + 2240c_2^2 - 1580c_2^3 + 261c_2^4 + 486c_2^5\\ +\left(176c_2^{1/2} - 488c_2^{3/2} + 584c_2^{5/2} + 159c_2^{7/2} + 162c_2^{9/2}\right)t_1\end{array}\right)c_4\end{array}\right)}{16c_2(1+2c_2)t_1^2\left(24 - 208c_2 + 131c_2^2 + 63c_2^3 + 54c_2^4 + \left(44c_2^{1/2} - 27c_2^{3/2} + 29c_2^{5/2} + 18c_2^{7/2}\right)t_1\right)}$$

$$\alpha_{0022} = \frac{-9\left(\left(-3 + 9 + c_2 - 42c_2^2\right)c_3^2 + \left(1 - 5c_2 + 4c_2^2 + 36c_2^3\right)c_4\right)}{16\left(c_2 - 5c_2^2 + 4c_2^3 + 36c_2^4\right)}$$

$$\alpha_{1111} = \frac{-9\sqrt{2}t_2\left(\begin{array}{r}\left(8 + 92c_2 - 109c_2^2 - 27c_2^3 + \left(45c_2^{1/2} - 9c_2^{3/2}\right)t_1\right)c_3^2\\ +(1+2c_2)\left(8 - 60c_2 + 55c_2^2 + 9c_2^3 + \left(8c_2^{1/2} - 23c_2^{3/2} + 3c_2^{5/2}\right)t_1\right)c_4\end{array}\right)}{8c_2(1+2c_2)\left(\left(-4 + 33c_2 - 26c_2^2 + 9c_2^3\right)t_1 + 40c_2^{1/2} - 157c_2^{3/2} + 102c_2^{5/2} + 27c_2^{7/2}\right)}$$

$$\alpha_{2002} = \frac{3\left(\begin{array}{r}\left(\begin{array}{r}-8 + 4c_2\left(47 - 51\sqrt{2}t_1t_2\right) + 27c_2^2\left(-85 + 16\sqrt{2}t_1t_2\right) + 2673c_2^3 + 486c_2^4\\ +8c_2^{1/2}\left(5t_1 - 36\sqrt{2}t_2\right) + c_2^{3/2}\left(959t_1 + 444\sqrt{2}t_2\right) + 99c_2^{5/2}t_1 + 162c_2^{7/2}t_1\end{array}\right)c_3^2\\ -(1 + c_2(-7 + 18c_2))\left(120 - 484c_2 + 429c_2^2 + 54c_2^3 + \left(160c_2^{1/2} - 41c_2^{3/2} + 18c_2^{5/2}\right)t_1\right)c_4\end{array}\right)}{8c_2\sqrt{2}t_2(1 + c_2(-7 + 18c_2))\left(\left(12 - 17c_2 + 18c_2^2\right)t_1 - 104c_2^{1/2} + 69c_2^{3/2} + 54c_2^{5/2} +\right)}$$

where

$$t_1 = \sqrt{-8 + 9c_2}$$

$$t_2 = \sqrt{2 - c_2 + \sqrt{c_2}\sqrt{-8 + 9c_2}}$$

References

1. Brouwer, D., Clemence, G.M.: Methods of Celestial Mechanics. Academic Press, New York (1961)
2. Meyer, K.R., Hall, G.R.: Introduction to Hamiltonian Dynamical Systems and the N-Body Problem. Springer, New York (1991)
3. Henrard, J.: Periodic orbits emanating from a resonant equilibrium. Celest. Mech. **1**(3–4), 427–466 (1970)
4. Pucacco, G., Marchesiello, A.: An energy-momentum map for the time-reversal symmetric 1:1 resonance with $Z_2 \times Z_2$ symmetry. Physica D **271**, 10–18 (2014)
5. Farquhar, R.W.: The utilization of halo orbits in advanced lunar operations. NASA technical note. NASA TN D-6365 (1971)
6. Farquhar, R.W., Karne, A.A.: Quasi-periodic orbits about the translunar libration point. Celest. Mech. **7**, 458–473 (1973)
7. Farquhar, R.W., Muhonen, D.P., Newman, C.R., Hueberger, H.S.: Trajectories and orbital maneuvers for the first libration-point satellite. J. Guid. Control Dyn. **3**(6), 549–554 (1980)
8. Richardson, D.L.: Halo orbit formulation for the ISEE-3 mission. J. Guid. Control Dyn. **3**(6), 543–548 (1980)
9. Farquhar, R.W.: The control and use of libration-point satellites. NASA CR-95948: 1-214 (1968)
10. Richardson, D.L.: Analytic construction of periodic orbits about the collinear points. Celest. Mech. **22**(3), 241–253 (1980)

11. Jorba, Á., Masdemont, J.: Dynamics in the center manifold of the collinear points of the restricted three-body problem. Physica D **132**(1–2), 189–213 (1999)
12. Qian, Y.J., Yang, X.D., Zhang, W., Zhai, G.Q.: Periodic motion analysis around the libration points by polynomial expansion method in planar circular restricted three-body problem. Nonlinear Dyn. **91**(1), 39–54 (2018)
13. Almeida, A.K.D., Prado, A.F.B.A., Yokoyama, T., Sanchez, D.M.: Spacecraft motion around artificial equilibrium points. Nonlinear Dyn. **91**(3), 1473–1489 (2018)
14. Mihai, P., Vladimir, C.: The domain of initial conditions for the class of three-dimensional halo periodical orbits. Acta Astronaut. **36**(4), 193–196 (1995)
15. Koon, W.S., Lo, M.W., Marden, J.E., Ross, S.D.: Dynamical Systems, the Three-Body Problem and Space Mission Design. California Institute of Technology, Pasadena (2006)
16. Xu, M., Xu, S.J.: J_2 invariant relative orbits via differential correction algorithm. Acta. Mech. Sin. **23**, 585–595 (2007)
17. Ferrari, F., Lavagna, M.: Periodic motion around libration points in the elliptic restricted three-body problem. Nonlinear Dyn. **93**(2), 453–462 (2018)
18. Howell, K.C., Pernicka, H.J.: Numerical determination of Lissajous trajectories in the restricted 3-body problem. Celest. Mech. **41**(1–4), 107–124 (1987)
19. Qian, Y.J., Yang, X.D., Jing, W.X., Zhang, W.: An improved numerical method for constructing halo/Lissajous orbits in a full solar system model. Chin. J. Aeronaut. **31**(6), 1362–1374 (2018)
20. Kolemen, E., Kasdin, N.J., Gurfil, P.: Multiple Poincaré sections method for finding the quasiperiodic orbits of the restricted three body problem. Celest. Mech. Dyn. Astron. **112**(1), 47–74 (2012)
21. Jorba, Á.: A methodology for the numerical computation of normal forms, centre manifolds and first integrals of hamiltonian systems. Exp. Math. **8**(2), 155–195 (1999)
22. Celletti, A.: Stability and Chaos in Celestial Mechanics. Springer, Berlin; published in association with Praxis Publishing Ltd., Chichester, ISBN: 978-3-540-85145-5 (2010)
23. Bucciarelli, S., Ceccaroni, M., Celletti, A., Pucacco, G.: Qualitative and analytical results of the bifurcation thresholds to halo orbits. Ann. Mat. **195**(2), 489–512 (2016)
24. Gómez, G., Mondelo, J.M.: The dynamics around the collinear eqiualibrium points of the RTBP. Physica D **157**, 283–321 (2001)
25. Celletti, A., Pucacco, G., Stella, D.: Lissajous and halo orbits in the restricted three-body problem. J. Nonlinear Sci. **25**, 343–370 (2015)
26. Ceccaroni, M., Celletti, A., Pucacco, G.: Halo orbits around the collinear points of the restricted three-body problem. Physica D **317**, 28–42 (2016)
27. Delshams, A., Masdemont, J., Roldan, P.: Computing the scattering map in the spatial Hill's problem. Discrete Contin. Dyn. Syst. Ser. B **10**(2–3), 455–483 (2008)